Articles

Contribution from the Department of Chemistry,
McMaster University, Hamilton, Ontario L8S 4M1, Canada

The Fluoro(hydrogen cyanide)xenon(II) Cation. Preparation of $HC{\equiv}NXeF^+AsF_6^-$: A Multinuclear Magnetic Resonance and Raman Spectroscopic Study

Adel A. A. Emara and Gary J. Schrobilgen*

Received July 30, 1991

The XeF^+ or $Xe_2F_3^+$ cations react with $HC{\equiv}N$ in anhydrous HF solvent to give the Lewis acid–base adduct cation $HC{\equiv}NXeF^+$. The $HC{\equiv}NXeF^+$ cation has been characterized in HF and BrF_5 solvents by ^{129}Xe, ^{19}F, $^{14,15}N$, ^{13}C, and ^1H NMR spectroscopy and has been characterized as its AsF_6^- salt in the solid state by low-temperature Raman spectroscopy. The scalar couplings, $^1J(^{129}Xe-^{14}N)$, $^2J(^{129}Xe-^{13}C)$, and $^3J(^{129}Xe-^1H)$, represent the first examples of couplings observed between these nuclides. The vibrational assignments of the ν(Xe–N) stretching and δ(XeNC) and δ(FXeN) bending modes have been aided by obtaining Raman spectra for natural-abundance ^{15}N- and ^{13}C-enriched $HC{\equiv}NXeF^+AsF_6^-$. The solution NMR and low-temperature Raman spectroscopic studies are consistent with a linear $C_{\infty v}$ structure for the $HC{\equiv}NXeF^+$ cation. The vibrational data together with the NMR chemical shifts indicate that the Xe–N bond is weakly covalent and are in agreement with recent theoretical calculations. NMR spectroscopic studies also show that solutions of $HC{\equiv}NXeF^+AsF_6^-$ in HF are extensively solvolyzed to give equilibrium concentrations of the $HC{\equiv}NH^+$ cation and XeF_2.

Introduction

While many examples of xenon bonded to oxygen or fluorine and of xenon bonded to other highly electronegative inorganic ligands through oxygen were synthesized immediately following the discovery of noble-gas reactivity,[1] over a decade had elapsed before an example with a ligating atom other than oxygen and fluorine, namely nitrogen, was synthesized[2] and two decades before the Xe–N bond in $FXeN(SO_2F)_2$ was definitively characterized in the solid state by X-ray crystallography and in solution by multinuclear magnetic resonance spectroscopy.[3] Other imidodisulfurylfluoride xenon–nitrogen-bonded species have since been definitively characterized using primarily NMR spectroscopy, namely, $Xe[N(SO_2F)_2]_2$,[4,5] $F[XeN(SO_2F)_2]_2^+$,[4,5] $XeN(SO_2F)_2^+AsF_6^-$,[6] and $XeN(SO_2F)_2^+Sb_3F_{16}^-$,[6] and the latter salt has also been characterized by single-crystal X-ray diffraction. The compound $Xe[N(SO_2CF_3)_2]_2$[7] has also been prepared and characterized and is the most thermally stable of the imido derivatives of xenon.

Recently, a significant extension of noble-gas chemistry, and in particular compounds containing noble-gas nitrogen bonds, has been achieved by taking advantage of the Lewis acid properties of noble-gas cations.[8] In view of the propensity of the XeF^+ cation to form strong fluorine bridges to counteranions in the solid state,[9] the XeF^+ cation may be regarded as having a significant Lewis acid strength. On the basis of photoionization studies, $HC{\equiv}N$ is one of the most oxidatively resistant ligands among the perfluoropyridines and nitriles we have investigated thus far (first adiabatic ionization potential, 13.80 eV[10]). The estimated electron affinity of XeF^+ (10.9 eV)[11] suggested that $HC{\equiv}N$ would be resistant to oxidative attack by the XeF^+ cation and that the $HC{\equiv}NXeF^+$ cation might have sufficient thermal stability to permit its spectroscopic characterization in solution and in the solid state. The reaction of XeF^+ with $HC{\equiv}N$ and the subsequent isolation and characterization of $HC{\equiv}NXeF^+AsF_6^-$ have been reported in our previous communication.[12] We subsequently reported that a large number of oxidatively resistant Lewis nitrogen bases can interact with XeF^+ to form Lewis acid–base cations with XeF^+. Included among these bases are alkanenitriles and pentafluorobenzenenitrile,[12] perfluoroalkanenitriles,[13] perfluoropyridines,[14] and *s*-trifluorotriazine.[13] The present paper provides a detailed account of the synthesis and structural characterization of the $HC{\equiv}NXeF^+$ cation by low-temperature Raman spectroscopy in the solid state and in solution by ^1H, ^{13}C, $^{14,15}N$, ^{19}F, and ^{129}Xe NMR spectroscopy. More recently the krypton(II) analogue $HC{\equiv}NKrF^+$[15] and $R_FC{\equiv}NKrF^+$ ($R_F = CF_3$, C_2F_5, n-C_3F_7)[13] have also been synthesized and characterized in this laboratory, representing the first examples of krypton–nitrogen bonds.

The present paper and previous communications outlining the syntheses of $HC{\equiv}NXeF^+AsF_6^-$[12] and $HC{\equiv}NKrF^+AsF_6^-$[15] have been complemented by a recent theoretical investigation of $HC{\equiv}NNgF^+$ (Ng = Kr, Xe) at the SCF level by determination of the properties of the atoms and bonds in these molecules using the theory of atoms in molecules.[16]

Results and Discussion

The reactions of $XeF^+AsF_6^-$ and $Xe_2F_3^+AsF_6^-$ with $HC{\equiv}N$ were carried out according to eqs 1 and 2 by combining stoi-

$$XeF^+AsF_6^- + HC{\equiv}N \rightarrow HC{\equiv}NXeF^+AsF_6^- \quad (1)$$

$$Xe_2F_3^+AsF_6^- + HC{\equiv}N \rightarrow HC{\equiv}NXeF^+AsF_6^- + XeF_2 \quad (2)$$

(1) Bartlett, N.; Sladky, F. O. In *Comprehensive Inorganic Chemistry*; Bailar, J. C., Emeleus, H. J., Nyholm, R., Trotman-Dickenson, A. F., Eds.; Pergamon Press: New York, 1973; Vol. 1, Chapter 6.
(2) LeBlond, R. D.; DesMarteau, D. D. *J. Chem. Soc., Chem. Commun.* **1974**, 555.
(3) Sawyer, J. F.; Schrobilgen, G. J.; Sutherland, S. J. *Inorg. Chem.* **1982**, *21*, 4064.
(4) Schumacher, G. A.; Schrobilgen, G. J. *Inorg. Chem.* **1983**, *22*, 2178.
(5) DesMarteau, D. D.; LeBlond, R. D.; Hossain, S. F.; Nothe, D. *J. Am. Chem. Soc.* **1981**, *103*, 7734.
(6) Faggiani, R.; Kennepohl, D. K.; Lock, C. J. L.; Schrobilgen, G. J. *Inorg. Chem.* **1986**, *25*, 563.
(7) Foropoulos, J.; DesMarteau, D. D. *J. Am. Chem. Soc.* **1982**, *104*, 4260.
(8) Schrobilgen, G. J. In *Synthetic Fluorine Chemistry*; Olah, G. A., Chambers, R. D., Prakash, G. K. S., Eds.; Wiley: New York, in press.
(9) Selig, H.; Holloway, J. H. *Top. Curr. Chem.* **1984**, *124*, 33.
(10) Dibeler, V. H.; Liston, S. K. *J. Chem. Phys.* **1968**, *48*, 4765.
(11) EA(XeF^+) = IP(Xe) + BE(XeF^+) − BE(XeF^+) = 12.1 + 0.86 − 2.1 = 10.9 eV.
(12) Emara, A. A. A.; Schrobilgen, G. J. *J. Chem. Soc., Chem. Commun.* **1987**, 1646.
(13) Schrobilgen, G. J. *J. Chem. Soc., Chem. Commun.* **1988**, 1506.
(14) Emara, A. A. A.; Schrobilgen, G. J. *J. Chem. Soc., Chem. Commun.* **1988**, 257.
(15) Schrobilgen, G. J. *J. Chem. Soc., Chem. Commun.* **1988**, 863.
(16) MacDougall, P. J.; Schrobilgen, G. J.; Bader, R. F. W. *Inorg. Chem.* **1989**, *28*, 763.

0020-1669/92/1331-1323$03.00/0

Table I. NMR Chemical Shifts and Spin–Spin Coupling Constants for the HC≡NXeF$^+$ Cation

	Chemical Shifts[a]		
$\delta(^{129}Xe)$	−1552 (−1570)	$\delta(^{15}N)^c$	−234.5 (230.2)[d]
$\delta(^{19}F)^b$	−198.7 (−193.1)	$\delta(^{13}C)^e$	104.1
$\delta(^{14}N)$	−235.1	$\delta(^{1}H)$	4.70 (6.01)[f]
	Coupling Constants (Hz)		
$^1J(^{129}Xe-^{19}F)$	6161 (6176)	$^2J(^{15}N-^{19}F)$	23.9 (23.9)
$^1J(^{129}Xe-^{14}N)$	332	$^2J(^{15}N-^{1}H)$	(13.0)
$^1J(^{129}Xe-^{15}N)$	471 (483)	$^3J(^{19}F-^{13}C)$	18
$^1J(^{14}N-^{13}C)$	22	$^3J(^{129}Xe-^{1}H)$	24.7 (26.8)
$^1J(^{13}C-^{1}H)$	308	$^4J(^{19}F-^{1}H)$	2.6 (2.7)[f]
$^2J(^{129}Xe-^{13}C)$	84		

[a] Samples were referenced externally at 24 °C with respect to the neat liquid references $XeOF_4$ (^{129}Xe), $CFCl_3$ (^{19}F), CH_3NO_2 (^{14}N and ^{15}N), and $(CH_3)_4Si$ (^{13}C and ^{1}H). A positive chemical shift denotes a resonance occurring to high frequency of the reference compound. The values in parentheses have been measured in BrF_5 solvent. [b] All ^{19}F spectra displayed a broad saddle-shaped feature at ca. −68 ppm arising from the partially quadrupole-collapsed $^1J(^{75}As-^{19}F)$ of the octahedral AsF_6^- anion. [c] Obtained from a 99.5% ^{15}N-enriched sample of HC≡NXeF$^+$AsF$_6^-$. [d] The sample was prepared and run at −50 °C in BrF_5 solvent by redissolving a solid sample of 99.5% ^{15}N-enriched HC≡NXeF$^+$AsF$_6^-$ that had been prepared in HF solvent. [e] Obtained from a 99.2% ^{13}C-enriched sample of HC≡NXeF$^+$AsF$_6^-$. [f] The sample was prepared and run at −50 °C in BrF_5 solvent by redissolving a solid sample of natural-abundance HC≡NXeF$^+$AsF$_6^-$ that had been prepared in HF solvent.

chiometric amounts of the reactants in anhydrous HF and warming to −20 to −10 °C to effect reaction and dissolution. The compound HC≡NXeF$^+$AsF$_6^-$ was isolated as a colorless microcrystalline solid upon removal of HF solvent under vacuum at −30 °C and was stable for up to 6 h at 0 °C. After HF removal at −30 °C following reaction 2, XeF_2 was observed in the Raman spectrum of the solid sample prior to pumping off XeF_2 at 0 °C ($\nu_1(\Sigma_g^+)$, 495 cm^{-1}). Solutions of HC≡NXeF$^+$AsF$_6^-$ in HF at ambient temperature slowly decompose over a period of 14 h. The solvolytic behavior of HC≡NXeF$^+$AsF$_6^-$ in anhydrous HF at room temperature has been compared with that of HC≡N.[17] The reactions were also conducted in SO_2ClF solvent at 0 °C, but owing to the low solubility of the reactants and product in this solvent, the reactions did not go to completion.[12]

NMR Spectroscopy. Structure of the HC≡NXeF$^+$ Cation in Solution. Every element in the HC≡NXeF$^+$ cation possesses at least one nuclide which is suitable for observation by NMR spectroscopy, namely, the spin-$^1/_2$ nuclei ^1H, ^{13}C, ^{15}N, ^{129}Xe, and ^{19}F and the spin-1 nucleus ^{14}N. Multinuclear magnetic resonance spectra were recorded for HC≡NXeF$^+$AsF$_6^-$ in HF and BrF_5 solvents for all six nuclei using natural-abundance and ^{13}C- and ^{15}N-enriched compounds. All possible nuclear spin–spin couplings have been observed (structure I and Table I), establishing the solution structure of the HC≡NXeF$^+$ cation. In the course of the present NMR study, the couplings $^1J(^{129}Xe-^{14}N)$, $^2J(^{129}Xe-^{13}C)$, and $^3J(^{129}Xe-^{1}H)$ were observed, representing the first examples of scalar couplings between these nuclides.

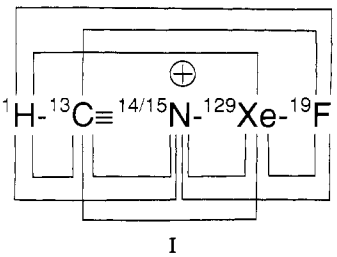

I

In prior studies of the imidodisulfurylfluoride derivatives of xenon(II), the low symmetry and resulting large electric field gradient (efg) at the ^{14}N nucleus in the trigonal planar −N(SO$_2$F)$_2$ group necessitated ^{15}N enrichment in order to observe xenon–nitrogen scalar couplings and nitrogen chemical shifts in FXeN(SO$_2$F)$_2$,[3] XeN(SO$_2$F)$_2^+$,[6] Xe[N(SO$_2$F)$_2$]$_2$,[4] and F[XeN(SO$_2$F)$_2$]$_2^+$[6] cations in SbF_5, BrF_5, and SO_2ClF solvents. In contrast, the axial symmetry of the HC≡NXeF$^+$ cation and resulting low efg at the ^{14}N nucleus, low viscosity of the HF solvent at −10 °C, and small quadrupole moment of ^{14}N serve to minimize quadrupole relaxation of the $^{129}Xe-^{14}N$ and $^{14}N-^{13}C$ couplings (see Nature of the Bonding in HC≡NXeF$^+$), allowing ready observation of the directly bonded $^{129}Xe-^{14}N$ and $^{14}N-^{13}C$ scalar couplings. However, in the higher viscosity solvent, BrF_5 (−58 °C), the $^{129}Xe-^{14}N$ and $^{14}N-^{13}C$ couplings are quadrupole-collapsed into single lines. Because they are generally obscured owing to quadrupolar relaxation caused by the ^{14}N nucleus, ^{15}N enrichment was required for the observation of scalar couplings between nitrogen and nondirectly bonded nuclei when the magnitudes of the couplings were small.

The ^{129}Xe NMR spectrum of natural-abundance HC≡NXeF$^+$ consists of a doublet arising from $^1J(^{129}Xe-^{19}F)$ in the Xe(II) region of the spectrum and is centered at −1570 ppm in BrF_5 solvent at −50 °C, $^1J(^{129}Xe-^{19}F)$ = 6176 Hz. The doublet ($^1J(^{129}Xe-^{19}F)$ = 6161 Hz) is centered at −1552 ppm in HF at −10 °C, and each doublet branch is further split into partially quadrupole-collapsed 1:1:1 triplets arising from the one-bond scalar coupling $^1J(^{129}Xe-^{14}N)$ = 332 Hz. The magnitude of $^1J(^{129}Xe-^{19}F)$ is comparable to directly bonded $^{129}Xe-^{19}F$ couplings of other xenon(II) compounds.[18-20] Failure to observe $^1J(^{129}Xe-^{14}N)$ in BrF_5 at −50 °C is attributed to the increased viscosity of BrF_5 relative to HF, leading to a longer molecular correlation time in the former solvent and quadrupole collapse of the $^{129}Xe-^{14}N$ scalar coupling. Carbon-13 enrichment (99.2%) led to further splitting into a doublet (84 Hz) on each peak in the ^{129}Xe NMR spectrum and is assigned to $^2J(^{129}Xe-^{13}C)$, representing the first reported example of a scalar coupling between ^{13}C and ^{129}Xe (Figure 1a).

Nitrogen-15 enrichment (99.5%) of the HC≡NXeF$^+$ cation was necessary because $^2J(^{14}N-^{1}H)$ and $^2J(^{19}F-^{14}N)$ could not be observed in natural-abundance HC≡NXeF$^+$AsF$_6^-$. In addition to observation of $^2J(^{15}N-^{1}H)$ and $^2J(^{19}F-^{15}N)$ in their respective ^{19}F, ^{15}N, and ^{1}H NMR spectra (vide infra), a well-resolved doublet of doublets on each doublet ($^1J(^{129}Xe-^{19}F)$) branch in the ^{129}Xe NMR spectrum of the ^{15}N-enriched cation was observed in both HF (−10 °C) and BrF_5 (−50 °C) solvents (Figure 1b). The fine structure is assigned to $^1J(^{129}Xe-^{15}N)$ (471 Hz in HF; 483 Hz in BrF_5) and $^3J(^{129}Xe-^{1}H)$ (24.7 Hz in HF; 26.8 Hz in BrF_5); the $^{129}Xe-^{1}H$ coupling was confirmed by a ^1H broad band decoupling experiment in the ^{129}Xe spectrum. Because of the smaller size of $^3J(^{129}Xe-^{1}H)$, quadrupolar line broadening by ^{14}N precludes observation of the latter coupling in the ^{129}Xe NMR spectrum of the natural-abundance cation. The magnitudes of $^1J(^{129}Xe-^{14}N)$ in the absence of quadrupole relaxation have been calculated for comparison with their observed values in HF solvent from the measured values of $^1J(^{129}Xe-^{15}N)$ using eq 3 [334 Hz (BrF_5 solvent at −50 °C) and 336 Hz (HF solvent at −10 °C; cf., 332 Hz, measured value)] and show the effect of residual quadrupolar relaxation on the measurement of $^1J(^{129}Xe-^{14}N)$ is negligible.

$$^1J(^{129}Xe-^{14}N) = {}^1J(^{129}Xe-^{15}N)(\gamma(^{14}N)/\gamma(^{15}N)) \quad (3)$$

The ^{19}F NMR spectra for natural-abundance and 99.2% ^{13}C-enriched HC≡NXeF$^+$AsF$_6^-$ in HF solvent at −10 °C and for 99.5% ^{15}N-enriched HC≡NXeF$^+$AsF$_6^-$ in BrF_5 solvent at −50 °C (Figure 2) consist of single ^{19}F environments with accompanying satellites that are attributed to $^1J(^{129}Xe-^{19}F)$. Under high resolution and in the absence of quadrupolar line broadening arising from ^{14}N, $^4J(^{19}F-^{1}H)$ = 2.6 (HF), 2.7 Hz (BrF_5), $^3J(^{19}F-^{13}C)$ = 24.7 (HF), 26.8 Hz (BrF_5), and $^2J(^{19}F-^{15}N)$ = 23.9

(17) Emara, A. A. A.; Schrobilgen, G. J. *Inorg. Chem.*, to be submitted for publication.

(18) Schrobilgen, G. J.; Holloway, J. H.; Granger, P.; Brevard, C. *Inorg. Chem.* **1978**, *17*, 980.
(19) Schrobilgen, G. J. In *NMR and the Periodic Table*; Harris, R. K., Mann, B. E., Eds.; Academic Press: London, 1978; Chapter 14, pp 439–454.
(20) Jameson, C. J. In *Multinuclear NMR*; Mason, J., Ed.; Plenum Press: New York, 1987, Chapter 18, pp 463–475.

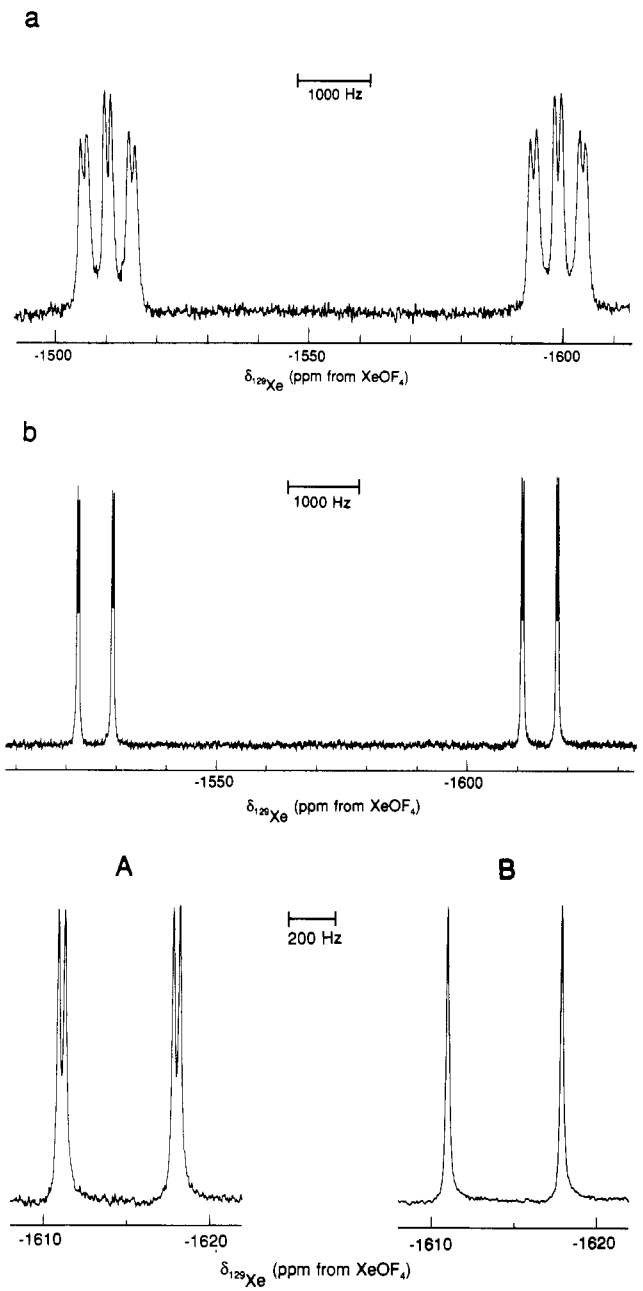

Figure 1. ^{129}Xe NMR spectra (69.563 MHz) of $HC{\equiv}NXeF^+AsF_6^-$: (a) 99.2% ^{13}C-enriched sample recorded in HF solvent at −10 °C; (b) 99.5% ^{15}N-enriched sample recorded in BrF_5 at −50 °C. Expansion A shows proton coupling, and expansion B is $\{^1H\}$-decoupled.

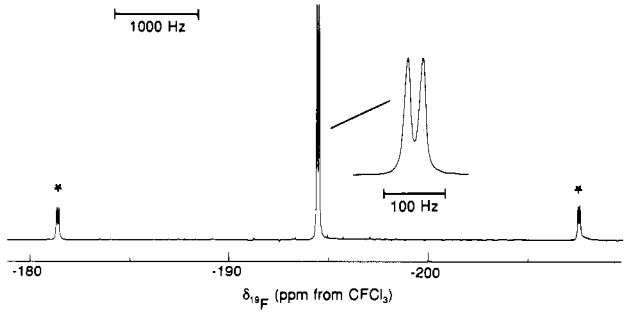

Figure 2. ^{19}F NMR spectrum (235.361 MHz) of 99.5% ^{15}N-enriched $HC{\equiv}NXeF^+AsF_6^-$ recorded in BrF_5 solvent at −50 °C. Asterisks denote ^{129}Xe satellites.

Hz were observed in the ^{15}N-enriched compounds (Table I). A broad, saddle-shaped feature (3150-Hz linewidth) also occurs at −68 ppm in these spectra and arises from the partially quadrupole-collapsed $^1J(^{75}As{-}^{19}F)$ coupling in the AsF_6^- anion.

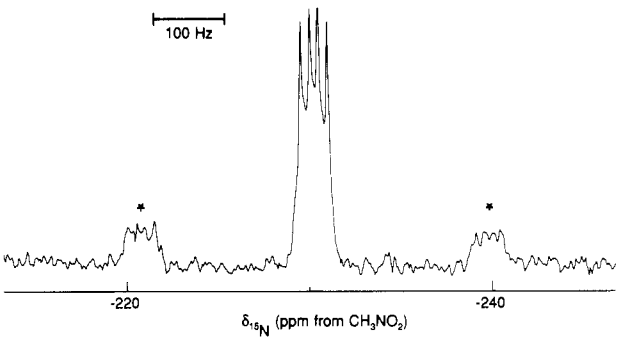

Figure 3. ^{15}N NMR spectrum (25.347 MHz) of 99.5% ^{15}N-enriched $HC{\equiv}NXeF^+AsF_6^-$ recorded in BrF_5 solvent at −50 °C. Asterisks denote ^{129}Xe satellites.

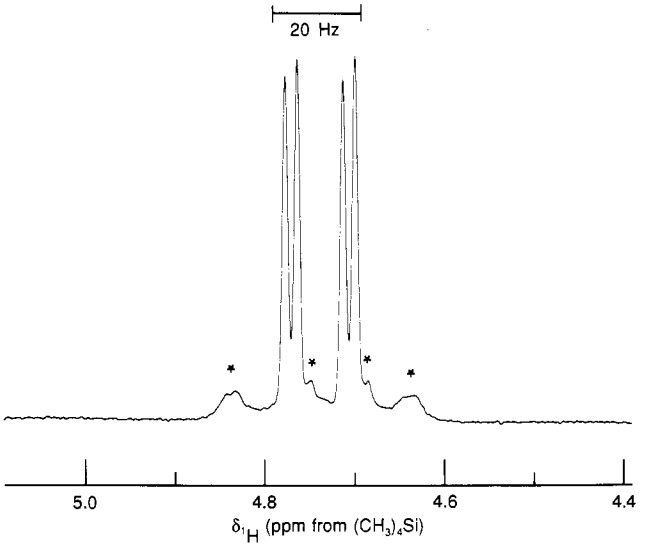

Figure 4. ^1H NMR spectrum (200.133 MHz) of 99.5% ^{15}N-enriched $HC{\equiv}NXeF^+AsF_6^-$ recorded in BrF_5 solvent at −50 °C. Asterisks denote ^{129}Xe satellites.

The ^{14}N and ^{15}N NMR spectra have been recorded for natural-abundance and 99.5% ^{15}N-enriched $HC{\equiv}NXeF^+AsF_6^-$, respectively. The ^{14}N NMR spectrum recorded in HF solvent at −10 °C consisted of a single line at −235.1 ppm with ^{129}Xe satellites ($^1J(^{129}Xe{-}^{14}N)$). The ^{15}N NMR spectrum of a 99.5%-enriched sample was also recorded under the same conditions in HF at −10 °C (−234.5 ppm) and in BrF_5 at −50 °C (−230.2 ppm) (Figure 3). The splitting pattern in the ^{15}N spectrum consisted of a doublet of doublets arising from $^2J(^{15}N{-}^{19}F)$ = 23.9 Hz (HF, BrF_5) and $^2J(^{15}N{-}^1H)$ = 13.0 Hz (BrF_5) (also observed in the ^1H and ^{19}F NMR spectra) and were accompanied by ^{129}Xe satellites ($^1J(^{129}Xe{-}^{15}N)$).

The ^1H NMR resonance of natural-abundance $HC{\equiv}NXeF^+AsF_6^-$ in BrF_5 solvent at −58 °C occurred at 6.01 ppm and consisted of a doublet with ^{129}Xe satellites, $^3J(^{129}Xe{-}^1H)$ = 2.7 Hz. The doublet is assigned to $^4J(^{19}F{-}^1H)$, but the two-bond $^{14}N{-}^1H$ coupling was not observed due to quadrupole relaxation by ^{14}N. However, $^4J(^{19}F{-}^1H)$ and $^2J(^{15}N{-}^1H)$ were both observed in the ^1H NMR spectrum for a 99.5% ^{15}N-enriched sample in BrF_5 solvent at −50 °C (Figure 4). The ^1H resonance in HF at −10 °C has also been observed for a natural-abundance sample and consisted of a single line at 4.70 ppm with ^{129}Xe satellites ($^3J(^{129}Xe{-}^1H)$).

The ^{13}C NMR resonance of $HC{\equiv}NXeF^+$ (Figure 5) for a 99.2% ^{13}C-enriched sample in HF solvent at −10 °C occurred at 104.1 ppm and consisted of a doublet ($^1J(^{13}C{-}^1H)$) of partially quadrupole-collapsed 1:1:1 triplets ($^1J(^{14}N{-}^{13}C)$ = 22 Hz) with ^{129}Xe satellites ($^2J(^{129}Xe{-}^{13}C)$) on each doublet branch.

Intense signals assigned to the $HC{\equiv}NH^+$ cation were also observed in the ^1H and ^{13}C NMR spectra and are attributed to equilibrium 4. The relative concentrations $[HC{\equiv}NH^+]/$

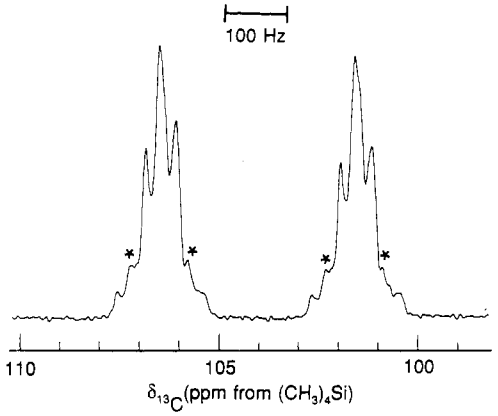

Figure 5. ^{13}C NMR spectrum (62.915 MHz) of 99.2% ^{13}C-enriched $HC{\equiv}NXeF^+AsF_6^-$ recorded in HF solvent at −10 °C. Asterisks denote ^{129}Xe satellites.

$[HC{\equiv}NXeF^+]$ measured in the ^1H NMR spectrum of an HF solution having an initial $HC{\equiv}NXeF^+AsF_6^-$ concentration of 2.18 M at −10 °C was 4:1. The proton chemical shift $\delta(^1H)$ 7.43 ppm and $^2J(^{15}N{-}^1H)$ = 18.6 Hz for the proton on carbon of a ^{15}N-enriched sample are in excellent agreement with the previously reported values for $HC{\equiv}NH^+$ in the $FSO_3H{-}SbF_5{-}SO_2$ solvent system.[21] In contrast to the previous work in $FSO_3H{-}SbF_5{-}SO_2$, the proton on nitrogen environment and $^1J(^{14,15}N{-}^1H)$ were not observed, which is presumably the result of proton exchange with HF solvent. Additional NMR parameters for the $HC{\equiv}NH^+$ cation are reported here for the first time: $\delta(^{13}C)$ 97.1 ppm; $^1J(^{13}C{-}^1H)$ = 324.6, $^1J(^{13}C{-}^{14}N)$ = 40.7, and $^1J(^{13}C{-}^{15}N)$ = 59.5 Hz. However, neither the ^{14}N nor ^{15}N spectra of the $HC{\equiv}NH^+$ cation could be observed, even after a relaxation delay of 30 s was applied in the ^{15}N spectrum. A previous determination of $\delta(^{15}N)$ in $FSO_3H{-}SbF_5{-}SO_2$ solvent by the INDOR method gave a value of 119.4 ppm relative to external aqueous NH_4^+[21] (chemical shift relative to neat external CH_3NO_2 is −240.3 ppm calculated from a $\delta(^{15}N)$ value of −359.7 ppm for aqueous $NH_4^+Cl^-$ relative to CH_3NO_2[4]).

Although significant equilibrium amounts of $HC{\equiv}NH^+$ are observed in the ^{13}C and ^1H NMR spectra, XeF_2 is not observed in the ^{19}F and ^{129}Xe NMR spectra even in the presence of an equimolar amount of XeF_2 as in reaction 2. The apparent absence of XeF_2 in the NMR spectra is presumed to result from chemical exchange involving trace amounts of XeF^+ and $Xe_2F_3^+$ as exchange intermediates arising from equilibria 4–7 and XeF_2. The

$$HC{\equiv}NXeF^+ + HF \rightleftharpoons HC{\equiv}NH^+ + XeF_2 \quad (4)$$

$$HC{\equiv}NXeF^+ \rightleftharpoons HC{\equiv}N + XeF^+ \quad (5)$$

$$XeF^+ + 2HF \rightleftharpoons XeF_2 + H_2F^+ \quad (6)$$

$$XeF^+ + XeF_2 \rightleftharpoons Xe_2F_3^+ \quad (7)$$

^{129}Xe NMR spectra of $HC{\equiv}NXeF^+AsF_6^-$ and $CH_3C{\equiv}NXeF^+AsF_6^-$ in HF at −10 °C have been reported previously[12] and clearly show that the ^{129}Xe line width of $HC{\equiv}NXeF^+AsF_6^-$ (84 Hz, center line of the triplet) compared to that of $CH_3C{\equiv}NXeF^+AsF_6^-$ (40 Hz, center line of the triplet) is significantly larger. This observation is consistent with the anticipated lower base strength of $HC{\equiv}N$ toward XeF^+ relative to that of $CH_3C{\equiv}N$, resulting in a greater degree of dissociation for $HC{\equiv}NXeF^+$ (equilibrium 5) and ensuing chemical exchange by means of equilibria 4, 6, and 7.

In the course of this study it has also been shown that XeF_2 displaces HF in its reaction with $HC{\equiv}NH^+AsF_6^-$ in HF or BrF_5 solvents according to the reverse of equilibrium 4. The ^{129}Xe NMR spectrum was recorded for the molar ratio $XeF_2/HC{\equiv}NH^+AsF_6^-$ = 2.47 at −15 °C in HF solvent (initial $[XeF_2]$ = 0.230 M) and gave the relative equilibrium concentrations $[XeF_2]/[HC{\equiv}NXeF^+]$ = 0.81. While the XeF_2 1:2:1 triplet (−1555 ppm; $^1J(^{129}Xe{-}^{19}F)$ = 5530 Hz) could be observed under these conditions, it was significantly exchange broadened (line width 2590 Hz) relative to that of $HC{\equiv}NXeF^+$ (−1555 ppm; $^1J(^{129}Xe{-}^{19}F)$ = 6156 Hz; $^1J(^{129}Xe{-}^{14}N)$ = 330 Hz; line width 110 Hz), indicating that XeF_2 was undergoing slow chemical exchange, presumably via equilibria 5–7. Because $HC{\equiv}NXeF^+AsF_6^-$ has a low solubility in HF at temperatures approaching −30 °C, an equilibrium mixture of $HC{\equiv}NH^+AsF_6^-$ and XeF_2 was also studied in BrF_5 solvent at −50 °C for the molar ratio $XeF_2/HC{\equiv}NH^+AsF_6^-$ = 2.17, giving $[XeF_2]/[HC{\equiv}NXeF^+]$ = 0.72 at equilibrium (initial $[XeF_2]$ = 0.314 M). In contrast, the XeF_2 triplet (−1666 ppm; $^1J(^{129}Xe{-}^{19}F)$ = 5629 Hz) was significantly sharper (line width 250 Hz), which is consistent with a lower degree of dissociation of $HC{\equiv}NXeF^+$ according to equilibrium 5 (−1573 ppm; $^1J(^{129}Xe{-}^{14}N)$ was quadrupole collapsed at low temperatures in BrF_5; line width 470 Hz).

Raman Spectroscopy. The low-temperature (−196 °C) Raman spectra of the crystalline product, isolated from the reaction of natural-abundance and ^{15}N- and ^{13}C-enriched $HC{\equiv}N$ with $XeF^+AsF_6^-$ in anhydrous HF solvent, are shown in Figures 6 and 7, and the observed frequencies, along with their assignments, are listed in Table II. The ^{13}C- (99.2%) and ^{15}N-enriched (99.5%) salts were prepared in order to aid in the assignments of the ν(XeN) stretching and δ(HCN), δ(CNXe), and δ(NXeF) bending frequencies. The isotopic shifts are given by the ratios $\Delta\lambda(^{14/15}N)/\lambda(^{14}N)$ and $\Delta\lambda(^{12/13}C)/\lambda(^{12}C)$, as described in ref 24, and are defined and listed in Table II.

The Raman spectra are consistent with the formation of $HC{\equiv}NXeF^+AsF_6^-$ in the solid state. The linear $HC{\equiv}NXeF^+$ cation is expected to give rise to $3N - 5 = 10$ normal modes belonging to the irreducible representations $4\,\Sigma^+ + 3\,\Pi$ under the point symmetry $C_{\infty v}$. All ten modes are predicted to be Raman and infrared active and consist of four stretching modes $\nu_1(\Sigma^+)$, ν(H–C); $\nu_2(\Sigma^+)$, ν(C≡N); $\nu_3(\Sigma^+)$, ν(Xe–F); and $\nu_4(\Sigma^+)$, ν(Xe–N) and three doubly degenerate bending modes $\nu_5(\Pi)$, δ(HCN); $\nu_6(\Pi)$, δ(CNXe); and $\nu_7(\Pi)$, δ(NXeF). Therefore, seven bands are expected in the Raman and infrared spectra of the $HC{\equiv}NXeF^+$ cation. In addition, the octahedral AsF_6^- anion is expected to give rise to three Raman-active vibrational bands under O_h symmetry, $\nu_1(a_{1g})$, $\nu_2(e_g)$, and $\nu_5(t_{2g})$. However, 28 bands as opposed to the predicted 13 from a consideration of free ion symmetries are observed in the Raman spectrum of $HC{\equiv}NXeF^+AsF_6^-$ (Table II). The disparity between the number of observed bands and the number predicted from a consideration of the free species is attributed to vibrational coupling within the unit cell and/or reduction of the free ion symmetries due to site symmetry effects. The removal of all degeneracies by lowering of the cation and anion site symmetries to C_{2v} or lower would result in 25 Raman-active bands; however, in the absence of a crystallographic space group for $HC{\equiv}NXeF^+AsF_6^-$, it has not been possible in the ensuing discussion to determine their site symmetries and thereby account for the additional splittings and assign their symmetry species in a rigorous manner.

Vibrational assignments were aided by comparison with the vibrational frequencies of $HC{\equiv}N$,[22] $FXeN(SO_2F)_2$,[3] $XeF^+AsF_6^-$,[25] $Xe_2F_3^+AsF_6^-$,[26] and $M^+AsF_6^-$,[23] where M is an alkali metal, and by recent theoretical calculations of the harmonic frequencies of the $HC{\equiv}NKrF^+$ cation.[27–30] The three fundamental stretching modes ν(Xe–F), ν(C≡N), and ν(C–H) are readily assigned by comparison with the Raman spectra of $HC{\equiv}N$ in the gas phase and $XeF^+AsF_6^-$, which are also listed in Table

(21) Olah, G. A.; Kiovsky, T. E. *J. Am. Chem. Soc.* **1968**, *90*, 4666.
(22) Allen, H. C.; Tidwell, E. D.; Plyler, E. K. *J. Chem. Phys.* **1956**, *25*, 302.
(23) Naulin, C.; Bougon, R. *J. Chem. Phys.* **1976**, *64*, 4155.
(24) Tsuboi, M. *Spectrochim. Acta* **1960**, *16*, 505.
(25) This work.
(26) Zalkin, A.; Ward, D. L.; Biagioni, R. N.; Templeton, D. H.; Bartlett, N. *Inorg. Chem.* **1978**, *17*, 1318.
(27) Hillier, I. H.; Vincent, M. A. *J. Chem. Soc., Chem. Commun.* **1989**, 30.
(28) Koch, W. *J. Chem. Soc., Chem. Commun.* **1989**, 215.
(29) Wong, M. W.; Radom, L. *J. Chem. Soc., Chem. Commun.* **1989**, 719.
(30) Dixon, D. A.; Arduengo, A. J. *Inorg. Chem.* **1990**, *29*, 970.

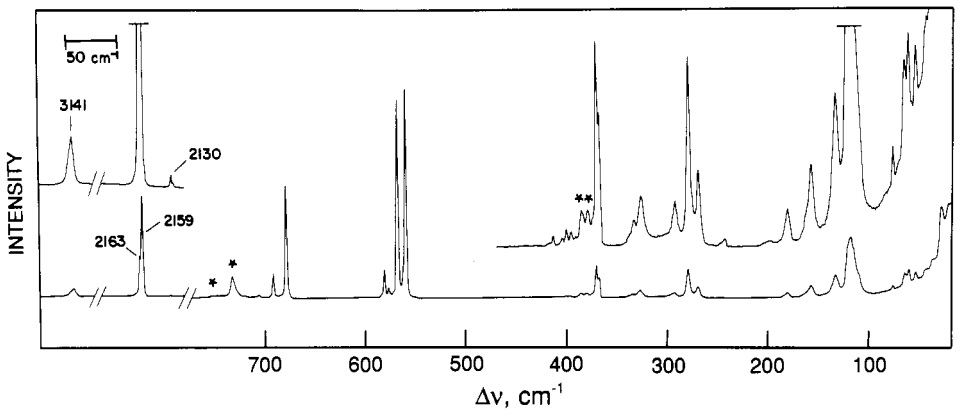

Figure 6. Raman spectrum of natural-abundance $HC{\equiv}NXeF^+AsF_6^-$ recorded at −196 °C. Asterisks denote FEP sample tube lines.

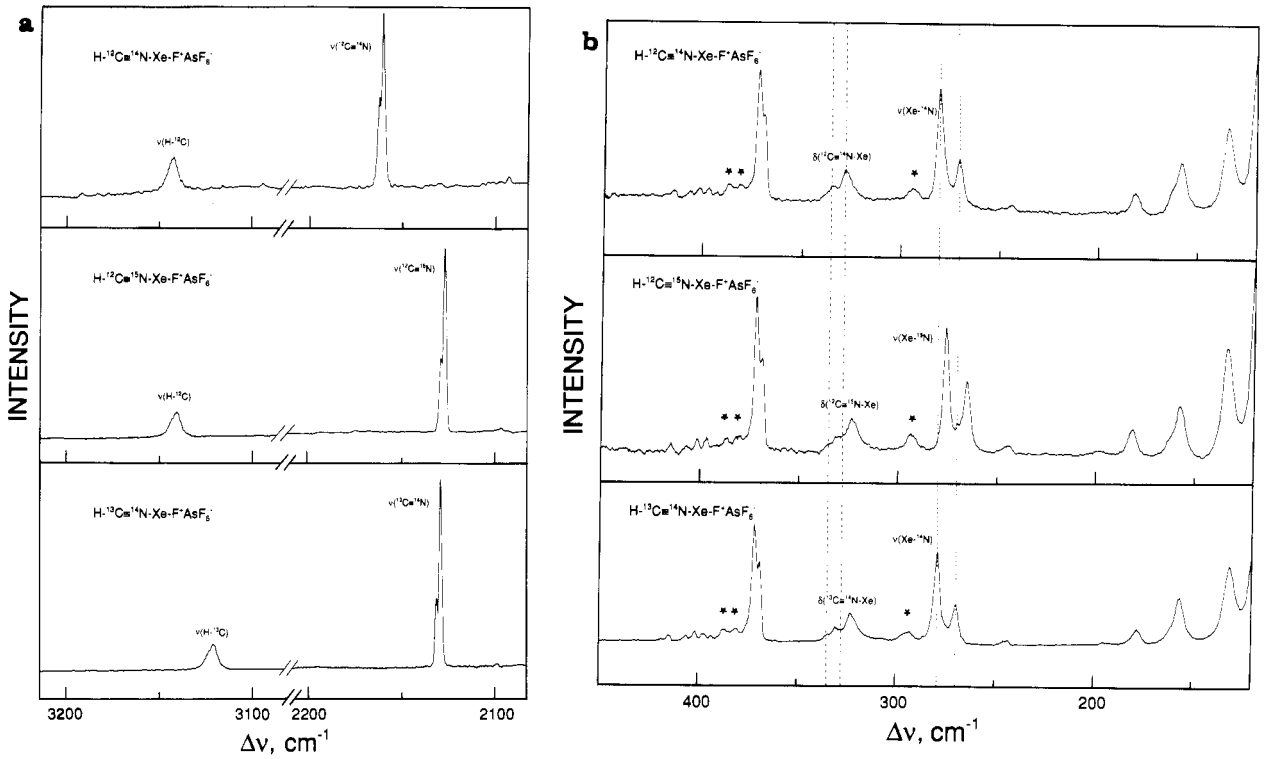

Figure 7. Raman spectra of natural-abundance, 99.2% ^{13}C-enriched, and 99.5% ^{15}N-enriched $HC{\equiv}NXeF^+AsF_6^-$, recorded at −196 °C: (a) 3200–2100-cm^{-1} region; (b) 400–100-cm^{-1} region. Asterisks denote FEP sample tube lines.

II. As the Xe–F and C–N stretching modes belong to the totally symmetric representation, Σ^+, their splittings can only be attributed to coupling of vibrational modes within the unit cell. The C–H stretching mode is also presumed to be factor-group split, but owing to its broadness, the anticipated splitting could not be resolved.

The most intense bands at 561 (100) and 569 (93) cm^{-1} are assigned to the Xe–F stretching frequency of the $HC{\equiv}NXeF^+$ cation and is characteristic of the terminal Xe–F bond in xenon(II) species of the type L–Xe–F (see Table III). The Xe–F stretching frequency can be used to assess the covalent nature of the Xe–L bond. The XeF^+ cation has been shown to be weakly coordinated to the anion by means of a fluorine bridge, and the Xe–F stretch has been shown to correlate with the degree of covalent character in the Xe---F bridge bond, decreasing with increasing base strength of the anion.[8] Consequently, the Xe–F stretching frequency is expected to increase as the xenon–nitrogen bond becomes more ionic and the terminal XeF bond becomes more covalent. A comparison of the Xe–F stretching frequency of $HC{\equiv}NXeF^+$ with other Xe–N-bonded species, XeF^+, and $Xe_2F_3^+$ allows one to assess the relative covalency of the Xe–N bond in the $HC{\equiv}NXeF^+$ cation. The stretching frequencies of the terminal Xe–F bond for F–Xe–L type derivatives are listed in Table III along with their Xe–F and Xe–L bond lengths when known. The $HC{\equiv}NXeF^+$ cation has the most ionic xenon–nitrogen bond when compared to previously reported Xe–N-bonded compounds for which vibrational data are available and is also in accord with our NMR findings (see above and Table III) and theoretical calculations at the SCF level (see Nature of the Bonding in

(31) Gillespie, R. J.; Schrobilgen, G. J. *Inorg. Chem.* **1976**, *15*, 22.
(32) Burgess, J.; Fraser, C. J. W.; McRae, V. M.; Peacock, R. D.; Russell, D. R. *J. Inorg. Nucl. Chem., Suppl.* **1976**, 183.
(33) Gillespie, R. J.; Netzer, A.; Schrobilgen, G. J. *Inorg. Chem.* **1974**, *13*, 1455.
(34) Schrobilgen, G. J. Unpublished work.
(35) Bartlett, N.; DeBoer, B. G.; Hollander, F. J.; Sladky, F. O.; Templeton, D. H.; Zalkin, A. *Inorg. Chem.* **1974**, *12*, 780.
(36) Bartlett, N.; Wechsberg, M.; Jones, G. R.; Burbank, R. D. *Inorg. Chem.* **1972**, *11*, 1124.
(37) Landa, B.; Gillespie, R. J. *Inorg. Chem.* **1973**, *12*, 1383.
(38) Syvret, R. G.; Schrobilgen, G. J. *Inorg. Chem.* **1989**, *28*, 1564.
(39) Birchall, T.; Myers, R. D.; deWaard, H.; Schrobilgen, G. J. *Inorg. Chem.* **1982**, *21*, 1068.
(40) Sanders, J. C. P.; Schrobilgen, G. J. Unpublished work.
(41) Agron, P. A.; Begun, G. M.; Levy, H. A.; Mason, A. A.; Jones, G.; Smith, D. F. *Science* **1963**, *139*, 842.

Table II. Raman Frequencies and Assignments for $HC{\equiv}NXeF^+AsF_6^-$, $[^{15}N]HC{\equiv}NXeF^+AsF_6^-$, and $[^{13}C]HC{\equiv}NXeF^+AsF_6^-$ and Related Compounds

frequency, cm^{-1} [a]									
HCN^b	$XeF^+AsF_6^-$ [c]	$HC{\equiv}NXeF^+AsF_6^-$	$[^{15}N]HC{\equiv}NXeF^+AsF_6^-$	$[^{13}C]HC{\equiv}NXeF^+AsF_6^-$	$\Delta\nu(^{14/15}N)$ [d,e]	$\Delta\nu(^{12/13}C)$ [d,e]	$\Delta\lambda(^{14/15}N)/\lambda(^{14}N)$ [f]	$\Delta\lambda(^{12/13}C)/\lambda(^{12}C)$ [f]	assgnt
3311		3141.9 (2)	3139.3 (3)	3121.0 (4)	−2.6	−20.9	−0.0016	−0.0133	$\nu_1(\Sigma^+)$, ν(CH)
2097		2162.1 (18)	2129.0 (17)	2130.8 (23)	−33.1	−31.3	−0.0304	−0.0287	$\nu_2(\Sigma^+)$, ν(CN)
		2160.0 (41)	2126.9 (47)	2128.7 (64)	−33.1	−31.3	−0.0304	−0.0288	
712									
	612 (61)	569.4 (93)	569.4 (97)	569.4 (97)	0.0	0.0	0.000	0.000	$\nu_5(\Pi)$, δ(HCN)
	610 (80)	561.2 (100)	561.2 (100)	561.2 (100)	0.0	0.0	0.000	0.000	$\nu_3(\Sigma^+)$, ν(XeF)
	608 (100)								
	602 (8)								
	347 sh								
	345 (58)								
									ν(F---XeF)
		334.7 (2)	330.6 (1)	334.3 (1)					
		327.9 (4)	323.4 (3)	330.6 (3)	−4.1	−4.1	−0.024	−0.024	?
		280.9 (14)	276.3 (11)	322.9 (5)	−4.5	−5.0	−0.027	−0.030	$\nu_4(\Sigma^+)$, ν(XeN)
		270.6 (6)	265.4 (6)	279.7 (14)	−4.6	−1.2	−0.032	−0.008	
	167 (2)			269.9 (6)	−5.2	−0.7	−0.038	−0.005	$\nu_6(\Pi)$, δ(CNXe)
	164 (5)								
	160 (7)								δ(F---XeF)
	150 (9)								
	147 (6)								
	142 (3)								
		181.2 (3)	181.2 (2)	177.8 (2)	0.0	−3.4	0.000	−0.037	$\nu_7(\Pi)$, δ(FXeN)
		163.0 sh	163 sh	163.3 sh	0	−1.7	0.00	−0.021	
		157.6 (6)	156.9 (5)	156.2 (7)	−0.7	−1.4	−0.009	−0.018	
		134.6 (10)	133.6 (9)	132.1 (11)	−0.8	−2.5	−0.015	−0.037	
		118.0 (20)	117.1 (18)	117.0 (24)	−0.9	−1.0	−0.015	−0.017	

frequency, cm^{-1} [a]			assgnt	
AsF_6^- [g]	$XeF^+AsF_6^-$ [c]	$HC{\equiv}NXeF^+AsF_6^-$	$O_h(AsF_6^-)$	$C_s(AsF_6^-)$
700	735 (20)		$\nu_3(t_{1u})$	A″
	730 (5)			A′
	723 (13)	707 (2)		A′
		693 (11)		
689	681 (56)	680 (49)	$\nu_1(a_{1g})$	A′
573		582 (12)	$\nu_2(e_g)$	A′
		577 (5)		A′
	465 (3)			
384	421 (11)		ν(As---F)	
		419 (<1), 415 (1)	$\nu_4(t_{1u})$	A′
		406 (1)		A′
		401 (2)		A″
375	386 (14)	397 (1), 392 (<1)	$\nu_5(t_{2g})$	A′
	378 (5)	372 (15), 370 (10)		A″
252				A″
		244 (1)	$\nu_6(t_{1u})$	A′
				A″
	73 (9)			A″
		111 (sh), 77 (2), 71 (1), 65 (6), 62 (8), 54 (5), 44 (2), 43 (3)	lattice modes	

[a] Raman spectra of all of the $HC{\equiv}NXeF^+AsF_6^-$ salts were recorded with FEP sample tubes at −196 °C using 514.5-nm excitation. Lines due to FEP have been deleted from the spectra. Values in parentheses denote intensities; sh denotes a shoulder. Data given are for the spectra depicted in Figures 6 and 7. [b] Reference 22. [c] Recorded at −196 °C; this work. [d] $\Delta\nu(^{14/15}N) = \nu(^{15}N) - \nu(^{14}N)$; $\Delta\nu(^{12/13}C) = \nu(^{13}C) - \nu(^{12}C)$. [e] The estimated precision of each value is ±0.4 cm^{-1}. [f] $\Delta\lambda(^{14/15}N) = \lambda(^{15}N) - \lambda(^{14}N)$; $\Delta\lambda(^{12/13}C) = \lambda(^{13}C) - \lambda(^{12}C)$, where $\lambda = 4\pi^2c^2\nu^2$, c is the velocity of light, and ν is the observed frequency (in cm^{-1}). [g] Reference 23.

Table III. Comparison of Xe–F Stretching Frequencies, Chemical Shifts, and Coupling Constants in F–Xe–L Derivatives

species[a]	XeF/XeL[b] bond lengths, Å	ν(Xe–F), cm^{-1}	NMR parameters[c] $^1J(^{129}Xe-^{19}F)$,[d] Hz	$\delta(^{129}Xe)$,[e,f] ppm	$\delta(^{19}F)$,[d,e] ppm	T, °C	ref
$XeF^+\cdots FSb_2F_{10}^-$[f]	1.82 (3)/2.34 (3)	619	7230	−574	−290.2	23[g]	18, 31, 32, 33
$XeF^+\cdots FAsF_5^-$[f]	1.873 (6)/2.212 (5)	610	6892	−869		−47	13, 25, 26, 31, 34
$(FXe)_2F^+$[f]	1.90 (3)/2.14 (3)	593	6740	−1051	−252.0	−62	18, 31, 33, 35
$CF_3C{\equiv}NXeF^+$			6397	−1337	−210.4	−63	13
$C_2F_5C{\equiv}NXeF^+$			6437	−1294	−212.9	−63	13
$n\text{-}C_3F_7C{\equiv}NXeF^+$			6430	−1294	−213.2	−63	13
$HC{\equiv}NXeF^+$	(1.904)/(2.421)	564	6181	−1569	−198.4[h]	−58	12
$CH_3C{\equiv}NXeF^+$[i]		560	6020	−1708	−185.5	−10	12
$s\text{-}C_3F_3N_2NXeF^+$		548	5932	−1862	−145.6	−50	13
			5909	−1808	−154.9	−5	
FO_2SOXeF	1.940 (8)/2.155 (8)	528	5830	−1666		−40	18, 33, 36, 37
cis/trans-$F_4OIOXeF$		527	5803/5910	−1824/−1720	−161.7[j]	0	38
					−170.1[j]	0	
$C_5F_5NXeF^+$		528	5926	−1922	−139.6	−30	14
$4\text{-}CF_3C_5F_4NXeF^+$		524	5963	−1853	−144.6	−50	14
$F_5TeOXeF$[k]		520		−2051	−151.0[l]	26	39, 40
$(FO_2S)_2NXeF$	1.967 (3)/2.200 (3)	506	5586	−1977	−126.1	−58	3, 4
			5664[l]	−2009[l]	−126.0[l]	−40	
XeF_2	1.977 (1.984)	496	5621	−1685	−184.3	−52	5, 13, 41

[a] Unless otherwise indicated, all cations have AsF_6^- as the counterion. [b] Bond lengths obtained from theoretical calculations are indicated in parentheses. [c] Spectra were obtained in BrF_5 solvent unless otherwise indicated. [d] The NMR parameters of XeF group, in particular $\delta(^{129}Xe)$, are very sensitive to solvent and temperature conditions; it is therefore important to make comparisons in the same solvent medium at the same or nearly the same temperature. [e] Referenced with respect to the neat liquids $XeOF_4$ (^{129}Xe) and $CFCl_3$ (^{19}F) at 24 °C; a positive sign denotes the chemical shift of the resonance in question occurs to higher frequency of (is more deshielded than) the resonance of the reference substance. [f] Table entries refer to the terminal fluorine on the xenon atom. [g] Recorded in SbF_5 solvent. [h] $\delta(^{19}F)$ measured in anhydrous HF solvent at −10 °C. [i] NMR parameters measured in HF solvent. [j] $\delta(^{19}F)$ meausured in SO_2ClF solvent at −40 °C. [k] NMR parameters measured in SO_2ClF solvent. [l] NMR parameters measured in SO_2ClF solvent at −50 °C.

$HC{\equiv}NXeF^+$). The latter calculations show that the reaction of the gas-phase XeF^+ ion with F^- to yield the difluoride results in an increase in the calculated Xe–F bond length of 0.1 Å, while the reaction of XeF^+ with $HC{\equiv}N$ causes the same bond length (calculated) to increase on average by only 0.016 Å.[16] Similar conclusions have been reached based on the high-frequency position of the Kr–F stretching frequency of $HC{\equiv}NKrF^+AsF_6^-$[15] and theoretical calculations for the $HC{\equiv}NKrF^+$ cation.[16,27-30]

The $\nu_1(\Sigma^+)$ C–H stretching vibration is assigned to a broad, weak band at 3142 (2) cm^{-1} and occurs at a significantly lower frequency than in gaseous $HC{\equiv}N$, i.e., 3311 cm^{-1},[22] and is consistent with coordination of the nitrogen lone pair to an electron pair acceptor. Two sharp lines at 2160 (41) and 2162 (18) cm^{-1} are assigned to the factor-group split $\nu_2(\Sigma^+)$ C≡N stretching mode and occur 63 cm^{-1} to higher frequency than the C≡N stretch of gaseous $HC{\equiv}N$. The shift to higher frequency upon coordination to XeF^+ is consistent with cation formation and with $HC{\equiv}N$ acting as a σ-electron pair donor to XeF^+. The C–H and C≡N stretching frequencies also exhibit the expected sensitivities to ^{13}C and ^{15}N substitution (Table II). The calculated changes in C–H and C≡N bond lengths parallel the observed shifts in the stretching frequencies in the $HC{\equiv}NXeF^+AsF_6^-$ salt (see Nature of the Bonding in $HC{\equiv}NXeF^+$).[16]

The assignments of the low-frequency cation bands arising from ν(Xe–N), δ(CNXe), and δ(FXeN) were aided by ^{15}N and ^{13}C isotopic enrichment. The relative order of the corresponding calculated frequencies for $HC{\equiv}NKrF^+$,[27-30] which are uniformly lower than in the xenon analogue, are consistent with the order arrived at for $HC{\equiv}NKrF^+$, i.e., ν(Xe–N) > δ(CNXe) > δ(FXeN).

The $\nu_3(\Sigma^+)$ Xe–N stretching vibration of the $HC{\equiv}NXeF^+$ cation is assigned to the weak, low-frequency lines 328 (4) and 335 (2) cm^{-1}, where the splitting is again attributed to vibrational coupling within the crystallographic unit cell. The assignment of the Xe–N stretch has been confirmed using ^{15}N and ^{13}C enrichment and results in relative shifts $\Delta\lambda(^{14/15}N)/\lambda(^{14}N)$ −0.027 and −0.024 for the two bands in the spectrum of $[^{15}N]HC{\equiv}NXeF^+AsF_6^-$ and $\Delta\lambda(^{12/13}C)/\lambda(^{12}C)$ −0.030 and −0.024 for $[^{13}C]HC{\equiv}NXeF^+AsF_6^-$ (Figure 7). The similarity between the $^{14}N/^{15}N$ and $^{12}C/^{13}C$ isotopic shifts is expected from a consideration of the form of the normal coordinate corresponding to $\nu_3(\Sigma^+)$. In the case of a heavy atom like Xe, the N and C displacements are expected to be essentially equal to one another and in the same but opposite sense to the small Xe displacement (cf. the actual form of the displacements in the normal coordinate corresponding to $\nu_1(\Sigma^+)$, the C–X stretch in $XC{\equiv}N$, where X = Cl, Br, or I[42]). The Xe–N frequency of the $HC{\equiv}NXeF^+AsF_6^-$ salt occurs at lower frequency than those of $FXeN(SO_2F)_2$ (422 cm^{-1})[3] and $Xe[N(SO_2F)]_2$ (386–413 cm^{-1}).[4] This is attributed to the greater covalent character of the Xe–N bonds in the imidodisulfurylfluoride derivatives, whereas the Xe–N bond of the $HC{\equiv}NXeF^+$ cation is among the most ionic Xe–N-bonded species presently known (the Xe–N bonds in $n\text{-}C_3F_7C{\equiv}NXeF^+$, $C_2F_5C{\equiv}NXeF^+$, and $CF_3C{\equiv}NXeF^+$ appear to be weaker on the basis of a comparison of their ^{129}Xe and ^{19}F chemical shifts; however, the vibrational spectra of these cations have not been recorded[13]). This is corroborated by the high-frequency position of the Xe–F stretch, which is among the highest of any F–Xe–L type species known where L is not bonded to the XeF group through fluorine.

The formally doubly degenerate bending mode $\nu_5(\Pi)$, δ(HCN) was not observed; this band is very weak in the Raman spectrum of gaseous $HC{\equiv}N$.[22] Although the frequency of the weak band at 707 (2) cm^{-1} is similar to δ(HCN) of gaseous $HC{\equiv}N$ (712 cm^{-1}), it was found to be insensitive to either ^{13}C or ^{15}N isotopic substitution and was accordingly assigned to an anion mode (vide infra). The assignments of the remaining doubly degenerate bending modes have been made with the aid of their $^{12}C/^{13}C$ and $^{14}N/^{15}N$ isotopic shift data. The presence of more than a single band for the δ(CNXe) and δ(FXeN) bending modes is ascribed to factor-group splitting and/or removal of the degeneracy by a cation site symmetry lower than $C_{\infty v}$.

The bending mode $\nu_6(\Pi)$, δ(CNXe) is assigned to lines at 271 (6) and 281 (14) cm^{-1} and exhibits the anticipated low-frequency shifts in the Raman spectra of $[^{13}C]HC{\equiv}NXeF^+AsF_6^-$ and $[^{15}N]HC{\equiv}NXeF^+AsF_6^-$, i.e., $\Delta\lambda(^{14/15}N)/\lambda(^{14}N)$ −0.038 and −0.032 and $\Delta\lambda(^{12/13}C)/\lambda(^{12}C)$ −0.005 and −0.008 (Figure 7). The $^{14}N/^{15}N$ dependence is large and is in fact similar to $\nu_1(\Sigma^+)$, the Xe–N stretching mode. The displacement of nitrogen from the

(42) Herzberg, G. *Infrared and Raman Spectra of Polyatomic Molecules*; Van Nostrand: New York, 1945; p 174.

molecular axis is expected to be large when bonded to a heavy atom while that of carbon is expected to be considerably less than the nitrogen displacement and in the opposite sense (cf. displacements for the normal modes in XC≡N[42]). The relatively small $^{12}C/^{13}C$ isotopic dependence for this mode is also supported by this qualitative description and is consistent with a smaller carbon displacement.

The bending mode ν_7(II), δ(FXeN) is expected at lower frequencies than δ(CNXe) and is assigned to the moderately intense bands at 118 (20) and 135 (10), 158 (6) and 181 (3) cm^{-1} by comparison with $XeF^+AsF_6^-$[25] and $Xe_2F_3^+AsF_6^-$,[26] where δ(FXe---F) are 155 (average) and 161 cm^{-1} (average), respectively, and $FXe-N(SO_2F)_2$,[3] where δ(FXeN) is 200 cm^{-1} (average). The FXeN bend of HC≡NXeF$^+$ is expected to be significantly lower than that of $FXeN(SO_2F)_2$. These modes also exhibit $^{14}N/^{15}N$ and $^{12}C/^{13}C$ isotopic dependences (Table II and Figure 7); however, no simple explanation for the relative magnitudes of each shift for each component of this doubly degenerate bend is presently available.

Although the AsF_6^- anion is not expected to be fluorine bridged to the HC≡NXeF$^+$ cation, the AsF_6^- anion exhibits 14 bands compared to the three Raman-active bands that are expected under O_h symmetry. Because the totally symmetric mode of AsF_6^-, $\nu_1(a_{1g})$, is not split, additional Raman-active bands are largely attributed to site symmetry lowering (15 Raman-active bands are expected for a site symmetry of C_{2v} or lower), although vibrational coupling in the unit cell may also contribute to the number of observed bands. The modes have been assigned under C_s symmetry by analogy with $XeF^+AsF_6^-$ (Table II), in which the O_h symmetry of the anion is reduced to C_s or lower symmetry by formation of a fluorine bridge to the anion. The vibrational frequencies for AsF_6^- under O_h symmetry have also been listed for comparison.

Lines occurring below 112 cm^{-1} exhibit no measurable shifts upon ^{13}C or ^{15}N substitution and have been assigned to lattice modes.

Nature of the Bonding in HC≡NXeF$^+$. Previous NMR studies of xenon(II) derivatives containing XeF groups bonded to oxygen or fluorine have shown that the NMR parameters measured in the ^{19}F and ^{129}Xe spectra can be used to assess relative covalent characters of the Xe–O, Xe---F bridge, and Xe–F terminal bonds.[18-20] In general, as the ionic character of the Xe–L (L = ligand atom) bond increases, the covalent character of the terminal Xe–F bond increases, increasing the formal charge on xenon. These trends are paralleled by decreases in $\delta(^{129}Xe)$ and increases in both $^1J(^{129}Xe-^{19}F)$ and $\delta(^{19}F)$ for the terminal XeF group. Table III provides the $\delta(^{129}Xe)$ and $\delta(^{19}F)$ chemical shifts and $^1J(^{129}Xe-^{19}F)$ for a number of xenon(II) compounds containing terminal Xe–F bonds for comparison with HC≡NXeF$^+$, showing that the Xe–F bond of HC≡NXeF$^+$ is second only to $R_FC{\equiv}NXeF^+$ (R_F = CF_3, C_2F_5, n-C_3F_7), $Xe_2F_3^+$, and XeF^+ in covalent character. Excluding fluorine bridging to xenon and the $R_FC{\equiv}NXeF^+$ cations,[13] the Xe–N bond of HC≡NXeF$^+$ is then among the weakest xenon–ligand bonds observed thus far. The XeF^+ character of the XeF group in HC≡NXeF$^+$ is supported by theoretical calculations of the efgs at the Xe nuclei in XeF^+ and HC≡NXeF$^+$,[16] which are found to differ by only 7%, in agreement with the experimental observation that the quadrupolar splitting in the ^{129}Xe Mössbauer spectra of HC≡NXeF$^+$ (40.2 ± 0.3 mm s^{-1}) is the same, within experimental error, as that obtained for the salt $XeF^+AsF_6^-$ (40.5 ± 0.1 mm s^{-1}).[43]

The observation of a well-resolved $^{129}Xe-^{14}N$ coupling in HF is the combined result of the low viscosity of HF, the axial symmetry, and the accompanying low efg at the ^{14}N nucleus.[44] The axial symmetry of the cation results in an asymmetry parameter $\eta = 0$ so that the efg at the ^{14}N nucleus is dominated by q_{zz}, the efg component along the C_∞ axis of the cation.[45] Consequently, the effect of the efg on quadrupolar relaxation of ^{14}N will only depend on q_{zz} and the molecular correlation time, τ_c. Coordination of XeF^+ to the nitrogen sp lone pair of HC≡N is expected to reduce q_{zz} significantly in the adduct cation, leading to a longer spin lattice relaxation time relative to the free base, further enhancing the possibility of observing $^1J(^{129}Xe-^{14}N)$ in the low-viscosity solvent, HF. The principal components of the efg tensor ($+z$ is in the direction H → N) at the nitrogen nuclei in HC≡N and HC≡NXeF$^+$ have been calculated, and the corresponding reduction in efg in going from HC≡N to HC≡NXeF$^+$ is 48%, in accord with our observation of $^1J(^{129}Xe-^{14}N)$ and $^1J(^{14}N-^{13}C)$ for HC≡NXeF$^+$ in HF solvent. The axial component of the efg tensor at the nitrogen nucleus is also halved upon the formation of HC≡NKrF$^+$.[16]

The difference in the magnitudes of the reduced coupling constants $^1K(Xe-N)$ in HC≡NXeF$^+$ (1.389×10^{22} N A^{-2} m^{-3}) and $FXeN(SO_2F)_2$ (0.949×10^{22} N A^{-2} m^{-3})[3,4,6] may be discussed using a previous assessment of the nature of bonding to xenon in solution for $FXeN(SO_2F)_2$. The Xe–N bond of $FXeN(SO_2F)_2$ is regarded as a σ-bond having sp^2 hybrid character. In high-resolution NMR spectroscopy spin–spin coupling involving heavy nuclides is generally dominated by the Fermi contact mechanism.[46] For Xe–N spin–spin couplings dominated by the Fermi contact mechanism, one-bond coupling constants can be discussed on the basis of the formalism developed by Pople and Santry.[47] In discussions of xenon–nitrogen scalar couplings in xenon(II) imidodisulfurylfluoride compounds,[6] the s-electron density at the xenon nucleus was assumed constant and a change in the hybridization at nitrogen accounted for changes in xenon–nitrogen spin–spin coupling. The dependence of xenon–nitrogen spin–spin coupling on nitrogen s-character in the xenon–nitrogen bond may also be invoked to account for the substantially larger $^1K(Xe-N)$ value observed for HC≡NXeF$^+$ than for xenon bonded to the trigonal planar nitrogen in $FXeN(SO_2F)_2$. A comparison of $^1K(Xe-N)$ for HC≡NXeF$^+$ with that of the trigonal planar sp^2 hybridized nitrogen atom in $FXeN(SO_2F)_2$ allows assessment of the relative degrees of hybridization of the nitrogen orbitals used in σ-bonding to xenon. The ratio $[^1K(Xe-N)_{sp}]/[^1K(Xe-N_{sp^2}]$ = 1.46 for the HC≡NXeF$^+$ cation and $FXeN(SO_2F)_2$ is in excellent agreement with the theoretical ratio, 1.50, calculated from the predicted fractional s-characters of the formally sp- and sp^2-hybridized nitrogen orbitals used in bonding to xenon in these compounds.

The Xe–N bond of the HC≡NXeF$^+$ cation may be thought of as a classical Lewis acid–base donor–acceptor bond. Implicit in this description of the Xe–N bond is a considerable degree of ionic character, which appears to be a dominant feature of the stability of the HC≡NXeF$^+$ cation. This premise has been supported and further illuminated by theoretical calculations on the HC≡NNgF$^+$ cations.[16,27-30] The ability of NgF^+ (Ng = Kr, Xe) cations to act as Lewis acids was shown to be related to the presence of holes in the valence shell charge concentrations of the Ng atoms that expose their cores.[16] The mechanism of formation of the Ng–N bonds in the adducts of NgF^+ with HC≡N is similar to the formation of a hydrogen bond; i.e., the mutual penetration of the outer diffuse nonbonded densities of the Ng and N atoms is facilitated by their dipolar and quadrupolar polarizations, which remove density along their axis of approach, to yield a final density in the interatomic surface that is only slightly greater than the sum of the unperturbed densities. Thus, not surprisingly, the KrF^+ and XeF^+ cations are best described as hard acids, which form weak covalent Ng–N adduct bonds as already noted in the context

(43) Schrobilgen, G. J.; Valsdóttir, N. Unpublished work.
(44) (a) Mason, J. In *Multinuclear NMR*; Mason, J., Ed.; Plenum Press: New York, 1987; Chapter 2, pp 11–13, 19. (b) Howarth, O. *Ibid.*, Chapter 5, pp 151–152.
(45) Lehn, J. M.; Kintzinger, J. P. In *Nitrogen NMR*; Witanowski, M., Webb, G. A., Eds.; Plenum Press: New York, 1973; Chapter 3, pp 81–84.
(46) (a) Jameson, C. J. In *Multinuclear NMR*; Mason, J., Ed.; Plenum Press: New York, 1987; Chapter 4, pp 116–118. (b) Jameson, C. J.; Gutowsky, H. S. *J. Chem. Phys.* **1969**, *51*, 2790. (c) Kunz, R. W. *Helv. Chim. Acta* **1980**, *63*, 2054. (d) Mason, J. *Polyhedron* **1989**, *8*, 1657. (e) Wrackmeyer, B.; Horchler, K. In *Annual Reports on NMR Spectroscopy*; Webb, G. A., Ed.; Academic Press: London, 1989; Vol. 22, p 261.
(47) Pople, J. A.; Santry, D. P. *Mol. Phys.* **1964**, *8*, 1.

of the present NMR and Raman spectroscopic studies. The energies of formation of these adducts are dominated by the large stabilizations of the Ng atoms that result from the increase in the concentration of charge in their inner quantum shells. The Ng–N bonds that result from the interaction of the closed-shell reactants NgF^+ and HC≡N actually lie closer to the closed-shell limit than do bonds formed in the reaction of NgF^+ with F^-. The calculated gas-phase energies of the reactions between the closed-shell species are −32.5 and −34.5 kcal mol^{-1} for Ng = Kr and Xe,[16] respectively, for

$$NgF^+ + HC{\equiv}N \rightarrow HC{\equiv}NNgF^+ \quad (8)$$

and −209.0 and −211.9 kcal mol^{-1} for

$$NgF^+ + F^- \rightarrow FNgF \quad (9)$$

The reactions of the gas-phase NgF^+ ions with F^- to yield the difluorides result in increases in the calculated Ng–F bond lengths of 0.1 Å, while their reaction with HC≡N causes the same bond lengths (calculated) to increase on average by only 0.016 Å.[16] The C–N bond of HC≡N is calculated to shorten by ~0.005 Å on forming the adduct, while the C–H bond is calculated to lengthen by 0.008 Å.[16] These predicted changes in bond length also correlate with the observed shifts in their corresponding stretching frequencies, ν(C≡N), increasing by 63 cm^{-1} and ν(C–H) decreasing by 169 cm^{-1} for $HC{\equiv}NXeF^+$.

A simple valence bond description may also be used to satisfactorily account for qualitative trends in bond lengths and associated spectroscopic parameters. The bonding in XeF_2 and $HC{\equiv}NXeF^+$ may be represented by valence bond structures II–VII, where structures IV and VII are the least important

$$\underset{\text{II}}{F\text{–}Xe^+\,F^-} \longleftrightarrow \underset{\text{III}}{F^-\,{}^+Xe\text{–}F} \longleftrightarrow \underset{\text{IV}}{F^-\,Xe^{2+}\,F^-}$$

$$\underset{\text{V}}{HC{\equiv}N\text{–}Xe^{2+}\,F^-} \longleftrightarrow \underset{\text{VI}}{HC{\equiv}N\,{}^+Xe\text{–}F} \longleftrightarrow \underset{\text{VII}}{HC{\equiv}N\,Xe^{2+}\,F^-}$$

contributing structures. The XeF_2 molecule has a formal bond order of $^1/_2$, and the Xe–F bond of $HC{\equiv}NXeF^+$ has a formal bond order (bo) of $^1/_2 \leq$ bo < 1; bo = 1 is approached only in the most weakly coordinated case of $FXe^+\cdots FSb_2F_{10}^-$. Unlike valence bond structures II and III of XeF_2 the analogous structures for $HC{\equiv}NXeF^+$, namely, structures V and VI, do not have equal weighting owing to the large buildup of formal positive charge on the Xe atom of structure V; consequently, structure VI dominates, resulting in an Xe–F bond having considerable covalent (XeF^+) character and a weak covalent Xe–N bond.

Experimental Section

Apparatus and Materials. All manipulations involving air-sensitive materials were carried out under anhydrous conditions on vacuum lines or in a drybox. Bromine pentafluoride and hydrogen fluoride were transferred on vacuum lines constructed largely from 316 stainless steel and nickel. Glass vacuum lines equipped with glass/Teflon grease-free stopcocks (J. Young) were used for the transfer of dry HC≡N and $H^{13}C{\equiv}N$.

Air-sensitive substances of low volatility and/or low thermal stability were transferred in a drybox equipped with cryogenic wells. Drybox moisture levels were routinely maintained at <0.1 ppm in a Vacuum Atmospheres Model DLX drybox.

Bromine pentafluoride (Ozark Mahoning Co.) was distilled into a $^3/_4$-in. Kel-F tube fitted with a Kel-F valve containing dry KF and purified by maintaining F_2 (2 atm) above the liquid for 5–7 days or until all the Br_2 and BrF_3 had reacted. The solvent was stored at room temperature under 1 atm of F_2 until used.

Anhydrous hydrogen fluoride (Harshaw Chemical Co.) was purified by treatment with 5 atm of F_2 gas in a nickel can for a period of at least 1 month, converting residual water to HF and O_2 gas. After the specified time period, anhydrous HF was vacuum distilled into a dry Kel-F storage vessel equipped with a Kel-F valve and stored at room temperature until used.

Hydrogen cyanide, HC≡N and $H^{13}C{\equiv}N$, was prepared by dropwise addition of H_2O to an equimolar mixture of KC≡N (British Drug House) or $K^{13}C{\equiv}N$ (Merck) and P_2O_5 (British Drug House).[47] The HC≡N/$H^{13}C{\equiv}N$ gas evolved was condensed into a glass U-tube at −196 °C and finally vacuum distilled into a glass vessel for drying over P_4O_{10}. In a typical reaction, 10.00 g, 154 mmol, of KC≡N (1.0098 g, 15.272 mmol, of $K^{13}C{\equiv}N$) was allowed to react to give 4.150 g of HC≡N and 0.428 g of $H^{13}C{\equiv}N$. The purities of the products were checked by recording the ^1H and ^{13}C NMR spectra of the neat liquids.

The salts $XeF^+AsF_6^-$ and $Xe_2F_3^+AsF_6^-$ were prepared as previously described.[33]

$HC{\equiv}NXeF^+AsF_6^-$, $[^{15}N]HC{\equiv}NXeF^+AsF_6^-$, and $[^{13}C]HC{\equiv}NXeF^+AsF_6^-$. The salt $HC{\equiv}NXeF^+AsF_6^-$ was prepared according to eqs 1 and 2. In typical preparations, two equal portions totalling 0.452 mmol of anhydrous HC≡N gas were condensed from a 54.41-mL bulb onto 0.1176 g (0.347 mmol) of $XeF^+AsF_6^-$ in 1.0–1.5 mL of HF solvent in a $^1/_4$-in. o.d. FEP tube outfitted with a Kel-F valve and previously cooled to −196 °C. The ambient pressure of anhydrous HC≡N gas that was condensed was 100–200 Torr to minimize dimer formation.[48] After the additions were complete, the mixture was warmed to −20 °C to effect dissolution and complete reaction. The product, $HC{\equiv}NXeF^+AsF_6^-$, was only sparingly soluble in HF at −30 °C, but as the temperature was gradually increased to −10 °C, the product dissolved. Slow cooling of the solution to −35 °C resulted in colorless needle-shaped crystals. The product was isolated by removal of HF solvent and excess HC≡N under vacuum at −30 °C. In the case of $Xe_2F_3^+AsF_6^-$, two equal portions of anhydrous HC≡N totaling 1.365 mmol were condensed onto 0.4722 g (0.9285 mmol) of $Xe_2F_3^+AsF_6^-$ in ca. 1.0–1.5 mL of anhydrous HF at −196 °C. The remainder of the procedure was identical to that used in the $XeF^+AsF_6^-$/HC≡N reaction except the product was pumped on for 6 h at 0 °C to remove XeF_2.

Nitrogen-15 (99.5%) and carbon-13-enriched (99.2%) $HC{\equiv}NXeF^+AsF_6^-$ were prepared according to the eq 1. In typical preparations, anhydrous hydrogen fluoride (1 mL) was condensed at −196 °C onto 0.1124 g (1.700 mmol) of $[^{15}N]KC{\equiv}N$ in a 9-mm FEP tube fitted with a Kel-F valve. The sample was agitated until all the $[^{15}N]KC{\equiv}N$ had dissolved. The resulting $[^{15}N]HC{\equiv}N$ was vacuum distilled, along with the HF solvent, onto 0.4631 g (1.365 mmol) of $XeF^+AsF_6^-$ in an $^1/_4$-in. o.d. FEP reaction tube/Kel-F valve assembly, followed by warming to −10 °C. A colorless solution resulted, which was rapidly cooled to −40 °C, whereupon HF and excess $[^{15}N]HC{\equiv}N$ were removed under vacuum. In a typical preparation of $[^{13}C]HC{\equiv}NXeF^+AsF_6^-$, 0.1498 g (2.266 mmol) of $[^{13}C]KC{\equiv}N$ and 0.5480 g (1.630 mmol) of $XeF^+AsF_6^-$ were used. The procedure was then the same as for the preparation of $[^{15}N]HC{\equiv}NXeF^+AsF_6^-$.

After HF removal, Raman spectra were obtained by running the spectra directly on the $^1/_4$-in. FEP reaction tube under 2 atm (ambient temperature) of dry N_2 gas. The ^{15}N- and ^{13}C-enriched samples were subsequently divided and transferred into 4-mm, 9-mm (FEP), and/or 5-mm glass sample tubes for NMR spectroscopy. During transfers, samples were maintained at low temperature by placing the sample tubes inside drilled copper blocks previously cooled to −196 °C in a cryogenic well inside the drybox. Natural-abundance samples for NMR spectroscopy were prepared by condensing a 30–35% molar excess of HC≡N onto the appropriate amount of $XeF^+AsF_6^-$ or $Xe_2F_3^+AsF_6^-$ in HF contained in the FEP NMR sample tube. In cases where the exact stoichiometry was desired, the sample was isolated as described above and redissolved in the appropriate solvent. All samples were dissolved at low temperature in either HF (−20 to −10 °C) or BrF_5 (−60 to −50 °C) and heat-sealed off from their Kel-F valves and stored at −196 °C until their NMR spectra could be recorded.

Nuclear Magnetic Resonance Spectroscopy. All NMR spectra were recorded unlocked (field drift < 0.1 Hz h^{-1}) with the use of Bruker AC-200 (4.6975 T) and WM-250 (5.8719 T) spectrometers.

Spectra were recorded on natural-abundance and 99.2% ^{13}C- and 99.5% ^{15}N-enriched samples in heat-sealed 9-mm o.d. or 4-mm o.d. FEP NMR tubes (HF and BrF_5 solvents) or in 5-mm precision Pyrex tubes (BrF_5 solvent; Wilmad Glass Co.) as described below. The FEP sample tubes were placed inside precision 10-mm o.d. or 5-mm o.d. glass NMR tubes before being placed in the probe.

The ^{129}Xe, ^{15}N, ^{14}N, and ^{13}C spectra were recorded at 5.8719 T in 9-mm FEP sample tubes (HF and BrF_5 solvent) on the same 10-mm probe (broad-banded over the frequency range 23–103 MHz) tuned to 69.563 (^{129}Xe), 18.075 (^{14}N), 25.347 (^{15}N), or 62.915 (^{13}C) MHz, respectively. Fluorine-19 spectra (235.361 MHz) were obtained on a 5-mm dual $^1H/^{19}F$ probe. Proton spectra (200.133 MHz) were recorded at 4.6975 T in HF solvent in 4-mm FEP sample tubes and in BrF_5 solvent in medium or thin-wall 5-mm o.d. precision glass sample tubes.

Xenon-129 NMR spectra of natural-abundance $HC{\equiv}NXeF^+AsF_6^-$ samples were recorded for spectral widths of 25 and 100 kHz with acquisition times of 0.164 and 0.082 s (17 000 and 150 000 scans), respectively, and a data point resolution of 6.10 Hz/pt. The ^{129}Xe NMR

(48) King, C. M.; Nixon, E. R. *J. Chem. Phys.* **1968**, *48*, 1685.

spectra of ^{13}C- and ^{15}N-enriched samples were recorded for spectral widths of 50 and 25 kHz (50000 and 1200-2500 scans), respectively, with acquisition times of 0.328 and 0.655 s and data point resolutions of 3.05 and 1.53 Hz/pt, respectively. Fluorine-19 NMR spectra were recorded for spectral widths of 50 and 100 kHz with acquisition times of 0.082 and 0.164 s and data point resolutions of 3.05 and 6.10 Hz/pt (4500 and 7500 scans), respectively. Nitrogen-15 and -14 NMR spectra were recorded for spectral widths of 25 and 10 kHz with acquisition times of 0.655 and 0.410 s and data point resolutions of 1.53 and 2.44 Hz/pt (1400 and 26000 scans), respectively. Carbon-13 NMR spectra were recorded for a spectral width of 15 kHz with an acquisition time of 0.541 s and data point resolution of 1.85 Hz/pt (3000 scans). Proton spectra were recorded for spectral widths of 800 Hz and 3 kHz with acquisition times of 5.12 and 2.80 s and data point resolutions of 0.098 and 0.357 Hz/pt (64 and 172 scans), respectively.

Pulse widths corresponding to bulk magnetization tip angles of ~90° were 22 (^{129}Xe), 2 (^{19}F), 49 (^{14}N), 35 (^{15}N), 7 (^{13}C), and 0.5 μs (^{1}H). No relaxation delays were applied except in the case of ^{15}N, where a relaxation delay of 10 s was applied. Line-broadening parameters used in exponential multiplication of the free induction decays were set equal to or less than their respective data point resolutions. All line shape functions were Lorentzian with the exception of the ^{1}H spectra and the ^{129}Xe NMR spectrum of $[^{13}C]HC{\equiv}NXeF^{+}AsF_6^{-}$; in these cases Gaussian line shapes were applied for resolution enhancement.

The respective nuclei were referenced externally to neat samples of $XeOF_4$ (^{129}Xe), $CFCl_3$ (^{19}F), CH_3NO_2 (^{14}N and ^{15}N), and $(CH_3)_4Si$ (^{13}C and ^{1}H) at 24 °C. Positive chemical shifts were assigned to resonances occurring to high frequency of the reference substance.[49]

For variable-temperature measurements, samples were kept cold (-196 or -78 °C) until immediately prior to their placement in the probe. They were generally warmed only enough to liquify and solubilize the contents and were then quickly placed in the precooled probe. Prior to data accumulation, the tubes were allowed to equilibrate in the probe for periods of several minutes while spinning. Temperatures were periodically checked by placing a copper-constantan thermocouple into the sampling region of the probe. Temperatures were considered to be accurate to within ±1 °C.

Raman Spectroscopy. A Coherent Model Innova 90 argon ion laser giving up to 3.5 W of power at 514.5 nm was used to excite the Raman spectra. The spectrometer was a Spex Industries Model 14018 double monochromator equipped with 1800 grooves/mm holographic gratings. Slit widths depended on the scattering efficiency of the sample, laser power, etc. and were set at 100-150 μm. An RCA C31034 phototube detector in conjunction with a pulse count system consisting of pulse amplifier, analyzer, and rate meter (Hamner NA-11, NC-11, and N-780 A, respectively) and a Texas Instruments Model FSOZWBA strip-chart recorder were used to record the spectra. The scanning rates used were 0.2 and 0.5 cm^{-1} s^{-1}. The typical power range used was between 0.7 and 1 W. The spectrometer was periodically calibrated by recording the discharge lines from an argon lamp over the spectral range of interest; all the Raman shifts quoted are estimated to be accurate to at least ±2 cm^{-1}, while the precision of each Raman shift measurement is estimated to be ±0.2 cm^{-1}.

Cylindrical $^{1}/_{4}$-in. FEP sample tubes were mounted vertically. The angle between the incident laser beam and sample tube was 45°, and Raman scattered radiation was observed at 45° to the laser beam (90° to the sample tube axis). Low-temperature spectra were recorded at -196 °C by mounting the sample vertically in an unsilvered Pyrex glass dewar filled with liquid nitrogen. All spectra were obtained directly in $^{1}/_{4}$-in. FEP reaction vessels. The spectrum of the FEP sample tube was nearly always observed; however, their prominence in the overall spectrum depended on the efficiency of the sample as a Raman scatterer and could be minimized by focusing the laser beam on the sample surface. Lines arising from FEP have been subtracted out of the spectra reported in the tables but not in the figures.

Acknowledgments. Research was sponsored by the U.S. Air Force Phillips Laboratory (formerly the Astronautics Laboratory), Edwards Air Force Base, under Contract F49260-87-C-0049 and by a Natural Sciences and Engineering Research Council of Canada operating grant.

(49) *Pure Appl. Chem.* **1972**, *29*, 627; **1976**, *45*, 217.

Contribution from the Department of Chemistry, University of Rochester, Rochester, New York 14627, and Eastman Kodak Company, Rochester, New York 14650

Multiple-State Emission from Platinum(II) Diimine Dithiolate Complexes. Solvent and Temperature Effects

Juan A. Zuleta,[1] Joanne M. Bevilacqua,[1] Julie M. Rehm,[2] and Richard Eisenberg*[,1]

Received August 6, 1991

The solvent and temperature dependence of the emission of Pt(diimine)(dithiolate) complexes is reported where diimine = 4,4'-dimethyl-2,2'-bipyridine (dmbpy) or 4,7-diphenyl-1,10-phenanthroline (dpphen) and dithiolate = 1-(ethoxycarbonyl)-1-cyanoethylene-2,2-dithiolate (ecda) or 1-(*tert*-butoxycarbonyl)-1-cyanoethylene-2,2-dithiolate (tbcda). In fluid solution at room temperature, a single emission band is observed at ~16670 cm^{-1} (600 nm) for the complexes Pt(dmbpy)(ecda) (**1**), Pt(dpphen)(ecda) (**2**), and Pt(dpphen)(tbcda) (**3**), which are studied in detail. The radiative quantum yields and lifetimes of the emission decrease with increasing solvent polarity for the three complexes. In DMF/CH_2Cl_2/MeOH the emission intensity for the complexes increases between 298 and 175 K with no change in the emission energy. Between 175 and 165 K the emission undergoes a red shift to ~15625 cm^{-1} (640 nm), corresponding to a rigidochromic effect, and below 140 K two new bands appear at higher energies (17000-18500 and 18600-19900 cm^{-1}). The latter bands have a relative separation of 1360 cm^{-1} and are assigned to a $\pi-\pi^*$ diimine transition on the basis of their observed lifetime and comparison with $PtCl_2$(diimine) analogues. Between 80 and 6 K, the lifetime of the 15625-cm^{-1} (640-nm) emission band increases, while, below 50 K, its emission intensity decreases with decreasing temperature, suggesting the presence of closely spaced excited states. From a kinetic analysis of the radiative quantum yield and lifetime data, the low-energy emission is assigned to a charge-transfer manifold of two emitting states separated by 50-60 cm^{-1}.

Introduction

Excited organic molecules almost always emit from the lowest excited state of a given multiplicity. This principle, known as Kasha's rule, does not always apply in the case of transition metal complexes, and a number of exceptions to the rule have been reported. The prime example of this group is $Ru(bpy)_3^{2+}$ (bpy = 2,2'-bipyridine) and its analogues, which Crosby and co-workers have shown to possess a metal-to-ligand charge-transfer (MLCT) manifold of three closely spaced, thermally equilibrated levels.[3] Another d^6 system of pseudooctahedral geometry is $CpRe(CO)_2L$ (Cp = η^5-cyclopentadienyl; L = pyridine, 4-phenylpyridine), which

(1) University of Rochester.
(2) Eastman Kodak Company.

(3) Hager, C. D.; Crosby, G. A. *J. Am. Chem. Soc.* **1975**, *97*, 7031.

0020-1669/92/1331-1332$03.00/0